*R*esearch in
*A*stronomy and
*A*strophysics

The updated Bulk Lorentz Factors of Gamma-Ray Burst X-Ray Flares

Shao-Qiang Xi[1], Shuang-Xi Yi[1,4], Yuan-Chuan Zou[2] and Fa-Yin Wang[3,4]

[1] College of Physics and Engineering, Qufu Normal University, Qufu 273165, China; *yisx2015@qfnu.edu.cn*

[2] School of Physics, Huazhong University of Science and Technology, Wuhan 430074, China

[3] School of Astronomy and Space Science, Nanjing University, Nanjing 210093, China; *fayinwang@nju.edu.cn*

[4] Key Laboratory of Modern Astronomy and Astrophysics (Nanjing University), Nanjing 210093, China

Abstract X-ray flares are the most common phenomena in the afterglow phase of gamma-ray bursts (GRBs) in the Swift era, and are known as a canonical component in X-ray afterglows. In this work, we constrain the Lorentz factor of X-ray flares with an updated sample. We extensively search for X-ray light curves showing flare and jet break simultaneously. A smooth broken power law function is used to fit the jet breaks in 11 GRBs. We also use a smooth broken power law function to fit the profile of X-ray flares, and the total number of the flares is 20. We obtain the lower and upper limits of Lorentz factor ($\Gamma_{\rm X}$) with the timescale, half-opening angle and mean luminosity of the X-ray flares for interstellar medium (ISM) and wind cases. The lower limits on $\Gamma_{\rm X}$ range from tens to a few hundred, and the upper limits are mainly about a few hundred. We also apply the limited Lorentz factor to test correlations of $\Gamma_0 - E_{\gamma,\rm iso}$ and $\Gamma_0 - L_{\gamma,\rm iso}$ for GRBs, and find X-ray flares in the ISM case are much more consistent with those of prompt emission than the wind case in a statistical sense for both correlations. X-ray flares are almost consistent with the trend in the correlations of $\Gamma_0 - E_{\gamma,\rm iso}(L_{\gamma,\rm iso})$ for prompt GRBs, indicating X-ray flares and prompt bursts may have the same physical origin.

Key words: gamma ray: bursts — radiation mechanism: non-thermal

1 INTRODUCTION

Gamma-ray bursts (GRBs) are the most luminous explosive events in the universe. The typical isotropic radiation energy of a GRB is about 10^{52} erg with a duration time of prompt gamma-rays emission ranging from a few milliseconds to thousands of seconds (Kouveliotou et al. 1993), followed by afterglow emissions in X-ray, optical and radio bands. The distribution of GRB prompt duration has been shown to be bimodal (Hurley 1989; Dezalay et al. 1992; Kouveliotou et al. 1993). Therefore, GRBs can be classified as short and long types, distinguished by a duration greater than or less than two seconds. According to the fireball model, prompt gamma-ray emission is supposed to be produced by internal shocks of collisions among shells, while the afterglows are from external shocks due to the interaction of an ultra-relativistic fireball shell with its surrounding medium (Meszaros & Rees 1993; Rees & Meszaros 1994; Mészáros & Rees 1997; Wu et al. 2003; Piran 2004; Zhang & Mészáros 2004; Yi et al. 2013). Many GRB afterglows have been detected, which could provide important clues about the properties of GRBs.

The relativistic motion of GRB ejecta has been confirmed (Piran 2004), but the value of the Lorentz factor is far from certain. There are many efforts to determine or constrain the Lorentz factor. Based on the fact that highly energetic GeV photons should not be absorbed by prompt MeV photons, one can derive a lower limit for GRBs in which GeV photons are observed (Fenimore et al. 1993; Zou et al. 2011). From the peak of the optical afterglow, one can obtain a weakly parameter dependent Lorentz factor (Mészáros & Rees 1997). Some other efforts have been proposed to derive upper or lower limits, such as thermal emission based on the fireball model (Pe'er et al.

2007), thermal emission with a timescale consistent with the light curve (Zou et al. 2015), the quiet stage of prompt emission (Zou & Piran 2010), the quiet stage of GeV photons (Nava et al. 2017), modeling the early afterglow based on the reverse-forward shock model (Sari & Piran 1999; Molinari et al. 2007; Jin & Fan 2007) and empirical relations containing the Lorentz factor (Liang et al. 2010; Ghirlanda et al. 2012; Lü et al. 2012; Fan et al. 2012).

X-ray flares are the most common phenomena in GRB X-ray afterglows, and they are also the most surprising discovery in the Swift era (Zhang et al. 2006; Nousek et al. 2006). X-ray flares are usually observed during the prompt emission phase and some occur at several days after the GRB trigger (Burrows et al. 2005; Fan & Wei 2005; Falcone et al. 2006, 2007; Wu et al. 2007; Chincarini et al. 2007, 2010; Yi et al. 2015, 2016). The temporal behavior and spectral properties of X-ray flares are different from underlying afterglow emissions, however they are consistent with those of prompt gamma-ray emissions. Mu et al. (2016) constrained the radiating regions of a group of X-ray flares with the characteristic timescale of the curvature effect and the Lorentz factor, and found radiation regions of the flares are within the regions of prompt gamma-rays and afterglows. Considering the same physical origin as prompt emission, X-ray flares should be a signal of restarting the GRB central engine or long-lasting central engine activities after the prompt gamma-rays.

In this paper, we constrain the Lorentz factor of X-ray flares with an updated sample. This paper is organized as follows. In Section 2, we present the selected GRB sample and method. In Section 3, we discuss the main results of our analysis. Conclusions and discussion are given in Section 4. A concordance cosmology with parameters $H_0 = 71\,\mathrm{km\,s^{-1}\,Mpc^{-1}}$, $\Omega_M = 0.30$ and $\Omega_\Lambda = 0.70$ is adopted in all parts of this work.

2 SAMPLE SELECTION AND METHOD

The initial Lorentz factor is a very important parameter for understanding the physics of GRBs. Some methods are proposed to constrain the initial Lorentz factor of GRBs. The most popular one is using the peak time of the early afterglow onset bump as the deceleration time of the external forward shock, and the Lorentz factor of the deceleration time is about half of the initial one (Sari & Piran 1999; Molinari et al. 2007; Liang et al. 2010). Considering that the reverse shock crossing time

almost corresponds to the deceleration time for a thin shell, Yi et al. (2015) calculated the initial Lorentz factor and obtained different coefficients for the theoretical Lorentz factor. More details can be seen in Section 2 of Yi et al. (2015). Liang et al. (2010) constrained the initial Lorentz factor of 20 GRBs with the deceleration feature in the early afterglow light curves, and found a tight correlation, $\Gamma_0 - E_{\gamma,\mathrm{iso}}$. This correlation was confirmed by Ghirlanda et al. (2012), Lü et al. (2012), Liang et al. (2013) and Yi et al. (2016). Ghirlanda et al. (2012) and Lü et al. (2012) also found a somewhat tighter correlation between Γ_0 and the isotropic mean γ-ray luminosity ($L_{\gamma,\mathrm{iso}}$). Interestingly, Fan et al. (2012) also confirmed some tight correlations, such as $\Gamma - L$, $E_\mathrm{p} - L$ and so on, and these correlations are consistent with relations between the analogous parameters predicted in the photospheric radiation model of prompt emission of GRBs. The time-resolved thermal radiation of GRB 090902B does follow the $\Gamma_0 - L$ correlation. Since both the prompt emission and X-ray flare have the same origin, X-ray flares may follow the $\Gamma_0 - E_{\gamma,\mathrm{iso}}(L_{\gamma,\mathrm{iso}})$ correlation. Therefore, we also apply a tight correlation to test whether X-ray flares and prompt emissions have the same origin.

Since the methods proposed to constrain the initial Lorentz factor of GRBs are not suitable for X-ray flares, we introduce two other methods to constrain the upper and lower limits on the Lorentz factor of X-ray flares in Yi et al. (2015). The lower limit on the Lorentz factor is

$$
\begin{aligned}
\Gamma_\mathrm{X} &> \left(\frac{T_\mathrm{decay}}{T_\mathrm{rise}}\right)^{\frac{1}{2}} \left[\frac{1}{2(1-\cos\theta_\mathrm{j})}\right]^{\frac{1}{2}} \\
&\approx \theta_\mathrm{j}^{-1}\left(\frac{T_\mathrm{decay}}{T_\mathrm{rise}}\right)^{\frac{1}{2}},
\end{aligned}
\tag{1}
$$

where θ_j is the half-opening angle, and T_decay and T_rise are the decaying timescale and rising timescale of the flare respectively, which were also seen by Wu et al. (2007). The upper limit on the Lorentz factor is

$$
\Gamma_\mathrm{X} \leq \left(\frac{L\,\sigma_T}{8\pi m_\mathrm{p} c^3 R_0}\right)^{\frac{1}{4}},
\tag{2}
$$

where L and R_0 are the total luminosity and initial radius of the flare outflow respectively. In calculations, $L_\mathrm{X} = 0.1\,L$ and $R_0 = 10^7$ cm are assumed, which is the same as in Jin et al. (2010).

From the above, in order to constrain the lower and upper Lorentz factors, the X-ray light curve should show both the flare emission and jet opening angle. In this

Table 1 Parameters of the Prompt and X-ray Afterglow Emissions

GRB	z	α_1	α_2	$T_{\rm j}$ (d)	$E_{\gamma,{\rm iso}}$ (erg)	$\theta_{\rm j}^{\rm ISM}$ (rad)	$\theta_{\rm j}^{\rm Wind}$ (rad)	Ref.
080210	2.64	0.86 ± 0.09	1.70 ± 0.18	0.136 ± 0.063	$5.13{\rm E}52 \pm 2.13{\rm E}52$	0.031 ± 0.005	0.042 ± 0.005	[1]
080810	3.35	0.91 ± 0.03	1.78 ± 0.07	0.107 ± 0.022	$3.00{\rm E}53 \pm 2.00{\rm E}53$	0.021 ± 0.002	0.024 ± 0.001	[2]
080928	1.692	1.08 ± 0.06	1.96 ± 0.12	0.141 ± 0.035	$2.82{\rm E}52 \pm 1.17{\rm E}52$	0.038 ± 0.004	0.053 ± 0.003	[1]
081008	1.9685	0.85 ± 0.05	1.91 ± 0.20	0.209 ± 0.066	$6.92{\rm E}52 \pm 1.67{\rm E}52$	0.038 ± 0.005	0.045 ± 0.004	[1]
100906A	1.727	0.76 ± 0.03	2.12 ± 0.08	0.153 ± 0.016	$3.34{\rm E}53 \pm 3.00{\rm E}52$	0.029 ± 0.001	0.029 ± 0.001	[3]
110801A	1.858	1.08 ± 0.06	1.75 ± 0.23	0.184 ± 0.104	$1.00{\rm E}53 \pm 2.00{\rm E}52$	0.035 ± 0.007	0.040 ± 0.006	[4]
121024A	2.298	0.89 ± 0.04	1.84 ± 0.23	0.539 ± 0.171	$2.51{\rm E}52 \pm 1.56{\rm E}52$	0.059 ± 0.007	0.072 ± 0.006	[5]
121211A	1.023	0.72 ± 0.12	1.52 ± 0.28	0.435 ± 0.285	$6.31{\rm E}51 \pm 5.38{\rm E}51$	0.078 ± 0.019	0.109 ± 0.018	[5]
130427B	2.78	0.92 ± 0.07	1.99 ± 0.36	0.209 ± 0.086	$3.16{\rm E}52 \pm 1.75{\rm E}52$	0.038 ± 0.006	0.052 ± 0.005	[5]
130606A	5.91	0.70 ± 0.28	1.78 ± 0.16	0.174 ± 0.046	$2.83{\rm E}53 \pm 5.2{\rm E}52$	0.022 ± 0.002	0.025 ± 0.002	[6]
140512A	0.725	0.81 ± 0.01	1.67 ± 0.05	0.213 ± 0.018	$1.17{\rm E}53 \pm 1.94{\rm E}52$	0.044 ± 0.001	0.046 ± 0.001	[7]

Reference: [1] Kann et al. 2011; [2] Liang et al. 2010; [3] Gorbovskoy et al. 2012; [4] Sakamoto et al. 2011; [5] Wei et al. 2014; [6] Golenetskii et al. 2013; [7] Golenetskii et al. 2014.

work, we identify jet breaks from afterglow light curves that show a transition from the normal decay phase (decay slope ~ -1) to a steeper phase (decay slope ~ -2), which is interpreted as a jet break (Rhoads 1999; Sari et al. 1999; Frail et al. 2001; Wu et al. 2004). We used a smooth broken power-law function to fit the jet breaks, which has the form

$$F(t) = F_0 \left[\left(\frac{t}{t_{\rm b}}\right)^{\alpha_1 \omega} + \left(\frac{t}{t_{\rm b}}\right)^{\alpha_2 \omega} \right]^{-\frac{1}{\omega}}, \qquad (3)$$

where α_1 and α_2 are the temporal slopes, $t_{\rm b}$ is the break time and ω represents the sharpness of the peak of the light curve component, for which usually $\omega = 3$ is applied. We obtain 11 GRBs with jet break features, which are presented in Table 1 and Figure 1. The half-opening angle can be calculated by the jet break time $T_{\rm j}$ and isotropic energy $E_{\gamma,{\rm iso}}$, for a homogeneous interstellar medium (ISM) case,

$$\theta_{\rm j}^{\rm ISM} = 0.076 \text{ rad } \left(\frac{T_{\rm j}}{1 \text{ day}}\right)^{3/8} \left(\frac{1+z}{2}\right)^{-3/8}$$
$$\times E_{\gamma,{\rm iso},53}^{-1/8} \left(\frac{\eta}{0.2}\right)^{1/8} \left(\frac{n}{1 \text{ cm}^{-3}}\right)^{1/8}, \quad (4)$$

and wind case,

$$\theta_{\rm j}^{\rm Wind} = 0.12 \text{ rad } \left(\frac{T_{\rm j}}{1 \text{ day}}\right)^{1/4} \left(\frac{1+z}{2}\right)^{-1/4}$$
$$\times E_{\gamma,{\rm iso},52}^{-1/4} \left(\frac{\eta}{0.2}\right)^{1/4} A_*^{1/4}, \qquad (5)$$

where the efficiency of prompt GRBs $\eta = 0.2$ and the wind parameter $A_* = 1$ are adopted. In this paper, we suppose the outflows are conical and the half-opening

angles of the outflows are a constant value, i.e., the half-opening angle of an X-ray flare jet is the same as that of a prompt jet.

As discussed above, the transition in the afterglow light curves from the normal decay phase (decay slope ~ -1) to a steeper phase (decay slope ~ -2) is best interpreted as a jet break. Under this criterion, only a few GRBs show a clear and similar jet break in optical and X-ray light curves simultaneously, and most of the values of $T_{\rm b}$ are calculated from the X-ray lightcurve. Wang et al. (2015b) found some cases in the selected sample have an acceptable achromatic break in both X-ray and optical bands, but there are still some in the sample that have a clear break at $T_{\rm b}$ in one band (e.g., X-rays), but do not have a break in another band (e.g., optical). They supposed the missing break is likely due to incomplete observational coverage before or after the break. We identified 11 GRBs with jet breaks in our X-ray flare sample, and the jet break times $T_{\rm j}$ are obtained by X-ray afterglow light curves. X-ray light curves are taken from the UK Swift/XRT website [1] (Evans et al. 2007, 2009). We used the smooth broken power law function to fit the jet breaks, and the best fitting results are shown in Figure 1 and Table 1. We obtain the break time $T_{\rm j}$, and the slopes α_1 and α_2 before and after the jet break respectively from the X-ray lightcurve. Since the type of GRB circumburst medium is uncertain, we consider two different types of surrounding media, ISM and wind cases. Along with the break time $T_{\rm j}$ and isotropic energy $E_{\gamma,{\rm iso}}$, we can calculate the half-opening angles from Equations (4) and (5). The half-opening angles are also presented in Table 1,

[1] *http://www.swift.ac.uk/xrt_curves/*
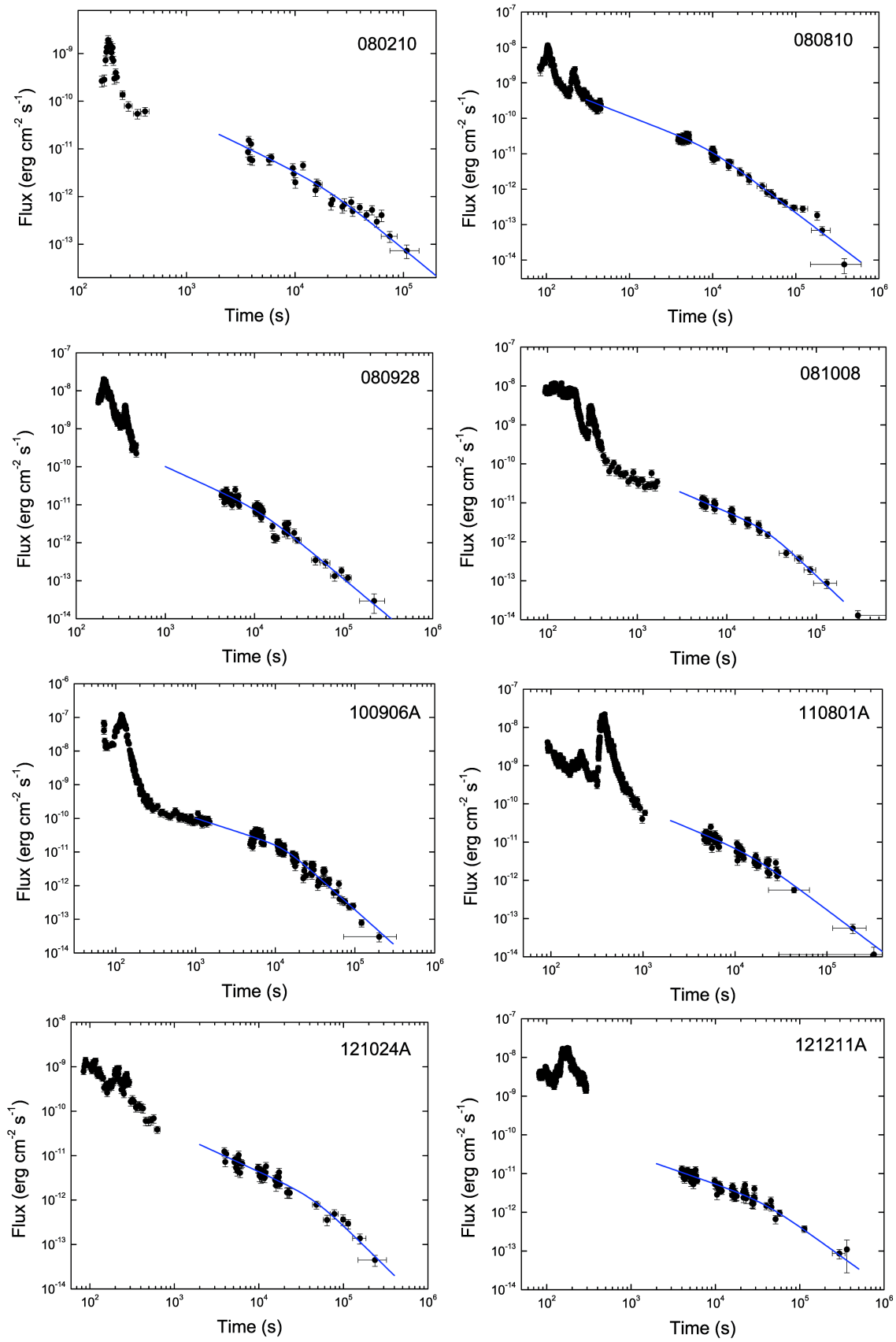
Fig. 1 GRB X-ray afterglows with jet break features. A smooth broken power-law function is applied to fit the break (*blue line*).
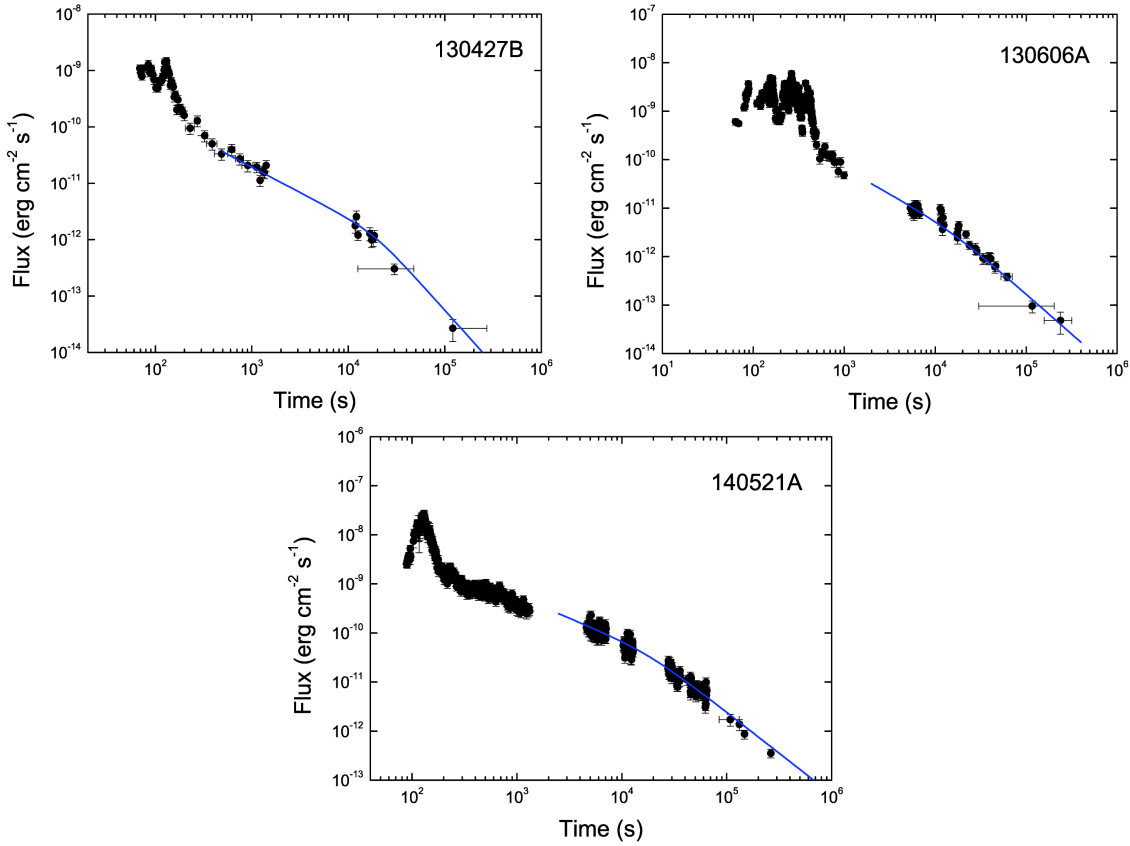
Figure 1 — *Continued.*

3 RESULTS

We also apply a smooth broken power law function to fit X-ray flares, which are followed by jet breaks. The method is very similar to the fitting method of Chincarini et al. (2007, 2010). We obtain the fitting results of X-ray flares, such as rising time, decaying time and fluence. More details can be seen in Yi et al. (2016), who analyzed all significant X-ray flares from the GRBs observed by Swift from 2005 April to 2015 March. The rising time, decaying time, duration and energy of X-ray flares are presented in Table 2. GRBs in our sample usually contain a single flare. However some of them have several flares. The total number of X-ray flares is 20. The isotropic energy of one flare is calculated by $E_{x,\mathrm{iso}} = 4\pi D_L^2 S_\mathrm{F}/(1 + z)$, where z is the redshift, D_L is the luminosity distance and S_F is the fluence of a flare. The duration of one flare is obtained by $T_{\mathrm{duration}} = T_{\mathrm{rise}} + T_{\mathrm{decay}}$. The mean luminosity of an X-ray flare

can be derived from $L_{x,\mathrm{iso}} = (1 + z)E_{x,\mathrm{iso}}/T_{\mathrm{duration}}$. Considering different types of circumburst media, we obtained the lower and upper limits on the Lorentz factor with the timescales, half-opening angles and mean luminosities of X-ray flares. The results are shown in Table 2 and Figure 2. The lower limits on Γ_X range from tens to a few hundred, and the upper limits are mainly about a few hundred.

We also investigate the correlations of $\Gamma_0 - E_{\gamma,\mathrm{iso}}$ and $\Gamma_0 - L_{\gamma,\mathrm{iso}}$ for GRBs and X-ray flares. We have plotted the correlations between the limits of Lorentz factors and energies of X-ray flares in Yi et al. (2015), and find these X-ray flares are almost consistent with the correlations of $\Gamma_0 - E_{\gamma,\mathrm{iso}}$ for the ISM case. Our results indicate that X-ray flares and GRBs may be caused by the same physical mechanism. The best fitting results of $\Gamma_0 - E_{\gamma,\mathrm{iso}}$ for ISM and wind are shown in Table 3. We also plot the correlation of $\Gamma_0 - L_{\gamma,\mathrm{iso}}$ for GRBs and X-ray flares, where the prompt data are taken from Liang et al. (2010, 2013) and Lü et al. (2012). Using equations (13) and (14) in Yi et al. (2015), we can obtain the initial Lorentz factor of GRBs for ISM and

and we apply the notation 'ISM' and 'Wind' in superscripts to distinguish the two types of surrounding media.

Table 2 Properties of GRB X-ray Flares

GRB	z	$T_{\rm rise}$ (s)	$T_{\rm decay}$ (s)	$T_{\rm dur}$ (s)	$E_{\rm x,iso}$ (erg)	Lower $\Gamma_{\rm X}^{\rm ISM}$	Lower $\Gamma_{\rm X}^{\rm Wind}$	Upper $\Gamma_{\rm X}$
080210	2.641	25.0	63.5	88.5	9.11E50 ± 8.41E49	51.1	38.3	278.8 ± 6.4
080810 (1)	3.35	25.1	27.9	53.0	3.79E51 ± 2.29E50	49.3	43.7	452.8 ± 6.8
080810 (2)	3.35	10.4	39.3	49.7	1.09E51 ± 1.28E50	91.0	80.7	336.8 ± 9.9
080928 (1)	1.692	59.8	141.2	201.0	6.46E51 ± 1.99E50	40.2	29.2	370.7 ± 2.9
080928 (2)	1.692	30.5	50.0	80.5	5.94E50 ± 4.03E49	33.6	24.3	256.5 ± 4.4
081008	1.9685	19.0	121.3	140.2	9.78E50 ± 5.13E49	66.3	55.8	252.9 ± 3.3
100906A	1.727	43.0	87.6	130.6	2.25E52 ± 9.1E50	49.6	49.4	563.7 ± 5.7
110801A (1)	1.858	21.7	30.3	51.9	3.24E50 ± 7.11E49	33.5	29.2	246.0 ± 13.5
110801A (2)	1.858	41.4	266.2	307.6	9.61E51 ± 2.62E50	71.9	62.7	368.0 ± 2.5
121024A (1)	2.298	27.7	41.9	69.5	3.02E50 ± 5.42E49	20.7	17.1	224.7 ± 10.1
121024A (2)	2.298	18.5	50.9	69.4	1.85E50 ± 4.24E49	27.9	23.0	198.8 ± 11.4
121211A	1.023	50.1	697.9	748.0	2.94E51 ± 8.22E49	47.7	34.2	219.1 ± 1.5
130427B	2.78	13.6	40.9	54.5	4.36E50 ± 5.53E49	45.2	33.4	261.7 ± 8.3
130606A (1)	5.91	7.1	6.1	13.2	1.02E51 ± 1.58E52	42.7	37.7	461.8 ± 1785.0
130606A (2)	5.91	88.3	20.6	108.9	8.2E51 ± 1.78E51	22.2	19.6	458.5 ± 24.8
130606A (3)	5.91	25.4	31.0	56.4	3.77E51 ± 5.31E50	50.9	44.9	445.0 ± 15.7
130606A (4)	5.91	18.1	125.0	143.2	9.64E51 ± 8.31E50	120.8	106.6	446.0 ± 9.6
130606A (5)	5.91	64.1	60.9	125.1	5.15E51 ± 5.59E50	44.8	39.6	394.3 ± 10.7
140512A (1)	0.725	28.4	48.5	76.9	8.04E50 ± 4.89E49	29.6	28.6	279.9 ± 4.3
140515A (2)	6.32	1570.4	12106.0	13676.3	5.63E51 ± 1.43E51	108.3	87.2	124.7 ± 7.9

Table 3 Results of linear regression analysis for initial Lorentz factor Γ_0 and isotropic energy $E_{\gamma,\rm iso}$ ($L_{\gamma,\rm iso}$). R is the Spearman correlation coefficient, P is the chance probability and δ is the dispersion of correlation.

Correlations	Expressions	R	P	δ
$\Gamma_0(E_{\gamma,\rm iso})$ ISM	$\log \Gamma_0 = (2.15 \pm 0.03) + (0.25 \pm 0.05) \times \log E_{\gamma,\rm iso\,52}$	0.83	$< 10^{-4}$	0.13
$\Gamma_0(E_{\gamma,\rm iso})$ Wind	$\log \Gamma_0 = (1.60 \pm 0.02) + (0.33 \pm 0.02) \times \log E_{\gamma,\rm iso\,52}$	0.95	$< 10^{-4}$	0.09
$\Gamma_0(L_{\gamma,\rm iso})$ ISM	$\log \Gamma_0 = (2.51 \pm 0.03) + (0.24 \pm 0.03) \times \log L_{\gamma,\rm iso\,52}$	0.86	$< 10^{-4}$	0.12
$\Gamma_0(L_{\gamma,\rm iso})$ Wind	$\log \Gamma_0 = (2.07 \pm 0.03) + (0.30 \pm 0.03) \times \log L_{\gamma,\rm iso\,52}$	0.90	$< 10^{-4}$	0.12

wind cases (solid dots are shown in Figs. 4 and 5). The mean isotropic luminosities of GRBs are calculated by $L_{\gamma,\rm iso} = (1 + z)E_{\gamma,\rm iso}/T_{90}$, where T_{90} is the duration of a GRB. We find the correlation between the limited Lorentz factor and the mean luminosity of X-ray flares in the ISM case is more consistent with that of prompt emission than the wind case in a statistical sense, and X-ray flares are almost consistent with the correlation of $\Gamma_0 - L_{\gamma,\rm iso}$ for prompt GRBs. The best fitting results of $\Gamma_0 - L_{\gamma,\rm iso}$ for ISM and wind are shown in Table 3.

As discussed above, the physical origin of the flares may be the same as that of prompt gamma-rays. One may estimate Γ_X by assuming that the X-ray flares follow the same $\Gamma_0 - E_{\gamma,\rm iso}$ relation. Therefore, we apply the correlation $\Gamma_0 - E_{\gamma,\rm iso}$ to estimate the Lorentz factor with the radiation energy of X-ray flares for the ISM and wind cases. The derived Lorentz factor is usually less than 100, almost the same as our lower lim-

its on the Lorentz factor of flares, which can be seen in Figure 3. The X-ray flare sample of Figure 3 is from Yi et al. (2015) and this work. Interestingly, X-ray flare candidates appear in short GRBs, and short GRB flares show similar observational properties to long ones. Yi et al. (2016) studied 468 bright X-ray flares, including short GRB flares, and found some tight correlations, such as rise time correlated with decay time and duration time anti-correlated with peak time of flares, indicating longer rise times are associated with longer decay times and broader flares peak at later times. These tight correlations suggest that the structures of the pulses among those flares are similar, indicating a possible universal physical origin of the flares. The common properties between solar flares and GRB X-ray flares are also compared in Yi et al. (2016), who found power-law distributions of energies, durations, peak fluxes and waiting times in GRB X-ray flares and solar flares. These distributions can be
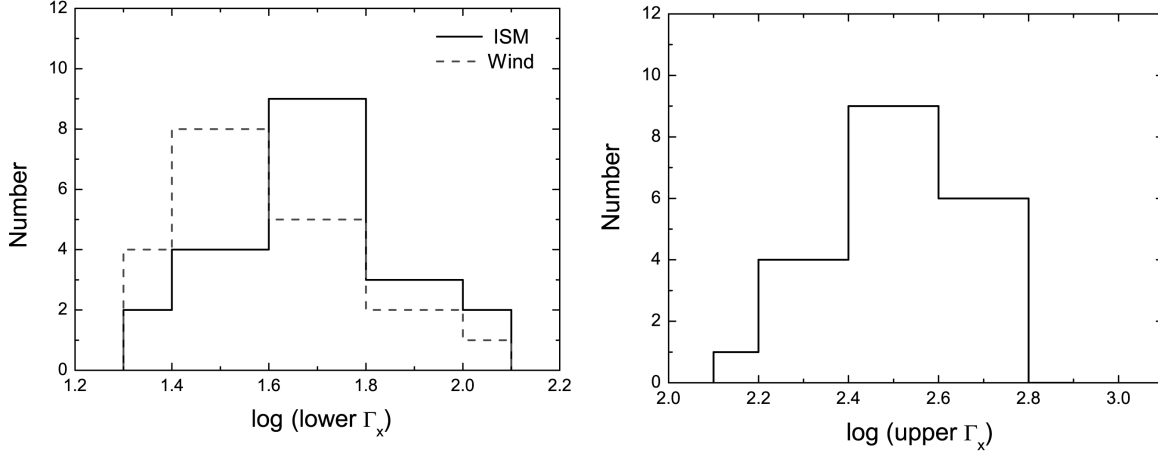
Fig. 2 Distribution of the limits on the Lorentz factor of X-ray flares. The lower limits on Γ_X range from tens to a few hundred for the ISM (*solid*) and wind (*dashed*) cases. The upper limits are mainly about a few hundred.
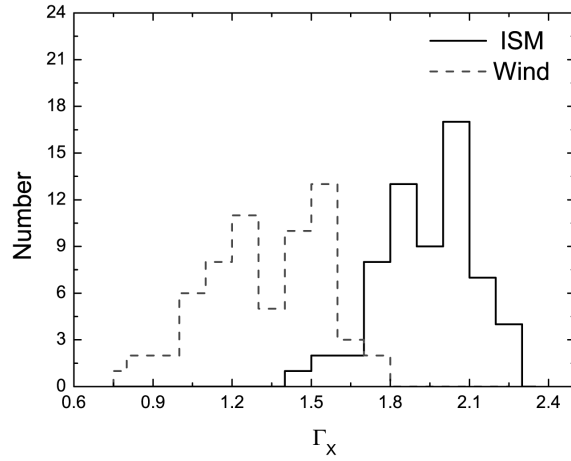
Fig. 3 The Lorentz factors of X-ray flares are calculated by the correlation of $\Gamma_0 - E_{\gamma,\mathrm{iso}}$ for ISM and wind cases. The estimated Lorentz factors are generally less than 100, and consistent with our lower limits on the Lorentz factors of X-ray flares. The flare sample is taken from Yi et al. (2015) and this work.

explained well by a fractal-diffusive, self organized criticality model and the relativistic jets of GRBs may be dominated by Poynting flux (Dai et al. 2006; Giannios 2006; Zhang & Yan 2011; Wang & Dai 2013; Wang et al. 2015a).

4 CONCLUSIONS AND DISCUSSION

In this work, we constrain the Lorentz factor of X-ray flares with an updated GRB sample, whose X-ray light curves show flares and jet breaks simultaneously. We use a smooth broken power law function to fit X-ray flares and jet breaks, and obtain 11 GRBs containing 20 X-ray flares. With the jet break time and isotropic energy,

we calculate the half-opening angle for ISM and wind cases. We obtain lower and upper limits on the Lorentz factor with the timescales, half-opening angles and the mean luminosities of X-ray flares. The lower limits on Γ_X range from tens to a few hundred and the upper limits are mainly about a few hundred. We also apply the limited Lorentz factor and isotropic energy to test the $\Gamma_0 - E_{\gamma,\mathrm{iso}}$ and $\Gamma_0 - L_{\gamma,\mathrm{iso}}$ correlations for GRBs. The results show that X-ray flares in the ISM case are more consistent with those of prompt emission than the wind case in a statistical sense for both $\Gamma_0 - E_{\gamma,\mathrm{iso}}$ and $\Gamma_0 - L_{\gamma,\mathrm{iso}}$ correlations. X-ray flares almost follow the trend shown by correlations of $\Gamma_0 - E_{\gamma,\mathrm{iso}}(L_{\gamma,\mathrm{iso}})$ for prompt GRBs,
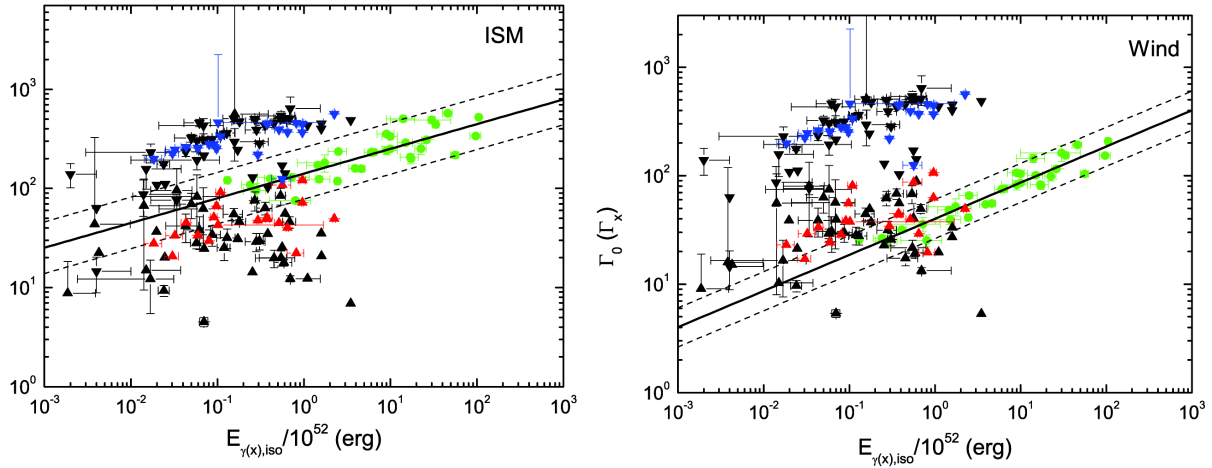
Fig. 4 The correlation of the Lorentz factor and isotropic radiation energy for prompt GRBs (*solid dots*) and X-ray flares (rest frame 0.3–10 keV, *triangles*). *Left panel*: the correlation for the ISM case. *Right panel*: the correlation for the wind case. The best fitting results are shown in Table 3. The black data are taken from Yi et al. (2015).
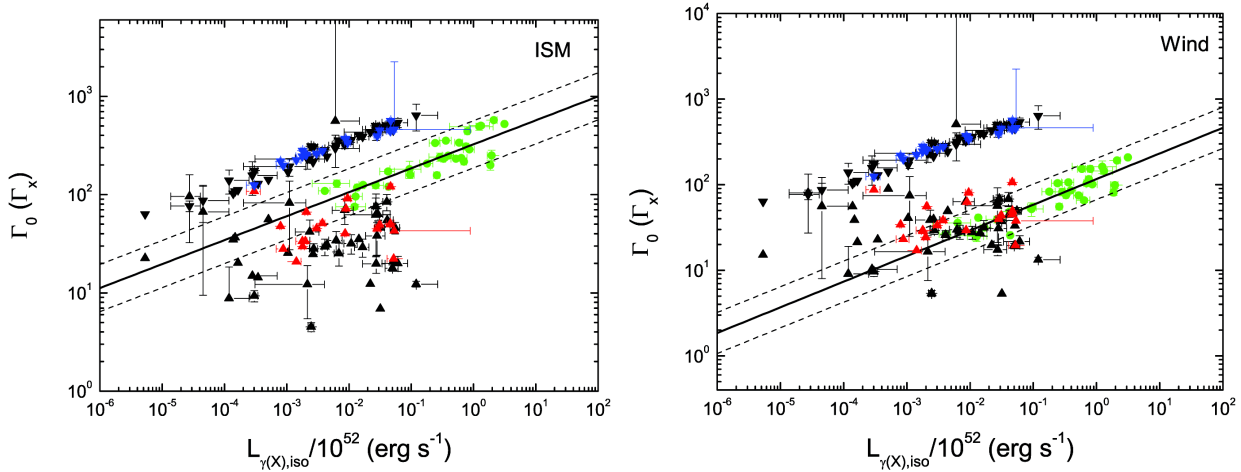
Fig. 5 Lorentz factor and mean isotropic luminosity of X-ray flares and prompt GRBs for two different cases. The symbols have the same meanings as in Fig. 4.

indicating X-ray flares and prompt bursts may have the same physical origin.

From Figures 4 and 5, one can see the X-ray flares are located in the bottom left. This clearly demonstrates that the Lorentz factors of the bulk emitting X-ray flares are different from the ejecta emitting prompt γ-rays, indicating the power and the Lorentz factor of the ejecta are decreasing from the central engine from a statistical perspective, and it may be also suitable for each single event.

With more accumulated data, and with time evolution of the Lorentz factor determined from X-ray flares, one may investigate how the statistical properties evolve

with time. These may be used to identify the fallback behavior of the progenitor, and consequently to determine the progenitor, though it is widely believed that long GRBs arise from collapsing massive stars. However, if one confirms that the peak luminosities of flares (or part of them) follow some specific behavior, this may indicate a diversity in classes of the progenitors. For instance, if some of them follow $t^{-5/3}$, which implies a merger origin for long GRBs, this may be a hint that some long GRBs are mergers of a neutron star and a white dwarf (or a main sequence star).

The estimated Lorentz factor may fail if the break in the afterglow is not from a jet break. As discussed in

Section 2, there are several GRBs with a non-achromatic break, which may not be explained by a jet break. Therefore, more reliable and robust methods are required to constrain the Lorentz factor. Until now, existing methods are mainly estimations and constraints. In the future, the most reliable method should be from spectral identification. With a more precise and broader band spectrum, one may identify the spectral line and determine the Lorentz factor directly. The strongest line should be from hydrogen, either Lyman series or Balmer series. With the boosting in the range of tens to hundreds, the observed lines are shifted to the keV band. Therefore, the enhancement of spectral resolution in the soft X-ray band will be definitely helpful for directly determining the Lorentz factors of X-ray flares as well as their afterglow. Using this approach, one can directly measure the dynamics. Another approach is to identify the unknown spectral lines in the optical band. If they are confirmed to be Doppler shifted from far-infrared lines corresponding to some specific enriched elements, one may also directly acquire the Lorentz factor. This may also need high resolution in the spectrum.

References

Burrows, D. N., Romano, P., Falcone, A., et al. 2005, Science, 309, 1833

Chincarini, G., Moretti, A., Romano, P., et al. 2007, ApJ, 671, 1903

Chincarini, G., Mao, J., Margutti, R., et al. 2010, MNRAS, 406, 2113

Dai, Z. G., Wang, X. Y., Wu, X. F., & Zhang, B. 2006, Science, 311, 1127

Dezalay, J.-P., Barat, C., Talon, R., et al. 1992, in American Institute of Physics Conference Series, 265, eds. W. S. Paciesas & G. J. Fishman, 304

Evans, P. A., Beardmore, A. P., Page, K. L., et al. 2007, A&A, 469, 379

Evans, P. A., Beardmore, A. P., Page, K. L., et al. 2009, MNRAS, 397, 1177

Falcone, A. D., Burrows, D. N., Lazzati, D., et al. 2006, ApJ, 641, 1010

Falcone, A. D., Morris, D., Racusin, J., et al. 2007, ApJ, 671, 1921

Fan, Y. Z., & Wei, D. M. 2005, MNRAS, 364, L42

Fan, Y.-Z., Wei, D.-M., Zhang, F.-W., & Zhang, B.-B. 2012, ApJ, 755, L6

Fenimore, E. E., Epstein, R. I., & Ho, C. 1993, A&AS, 97, 59

Frail, D. A., Kulkarni, S. R., Sari, R., et al. 2001, ApJ, 562, L55

Ghirlanda, G., Nava, L., Ghisellini, G., et al. 2012, MNRAS, 420, 483

Giannios, D. 2006, A&A, 455, L5

Golenetskii, S., Aptekar, R., Mazets, E., et al. 2013, GRB Coordinates Network, 14808, 1

Golenetskii, S., Aptekar, R., Frederiks, D., et al. 2014, GRB Coordinates Network, 16265, 1

Gorbovskoy, E. S., Lipunova, G. V., Lipunov, V. M., et al. 2012, MNRAS, 421, 1874

Hurley, K. 1989, Annals of the New York Academy of Sciences, 571, 442

Jin, Z. P., & Fan, Y. Z. 2007, MNRAS, 378, 1043

Jin, Z.-P., Fan, Y.-Z., & Wei, D.-M. 2010, ApJ, 724, 861

Kann, D. A., Klose, S., Zhang, B., et al. 2011, ApJ, 734, 96

Kouveliotou, C., Meegan, C. A., Fishman, G. J., et al. 1993, ApJ, 413, L101

Liang, E.-W., Yi, S.-X., Zhang, J., et al. 2010, ApJ, 725, 2209

Liang, E.-W., Li, L., Gao, H., et al. 2013, ApJ, 774, 13

Lü, J., Zou, Y.-C., Lei, W.-H., et al. 2012, ApJ, 751, 49

Meszaros, P., & Rees, M. J. 1993, ApJ, 405, 278

Mészáros, P., & Rees, M. J. 1997, ApJ, 476, 232

Molinari, E., Vergani, S. D., Malesani, D., et al. 2007, A&A, 469, L13

Mu, H.-J., Lin, D.-B., Xi, S.-Q., et al. 2016, ApJ, 831, 111

Nava, L., Desiante, R., Longo, F., et al. 2017, MNRAS, 465, 811

Nousek, J. A., Kouveliotou, C., Grupe, D., et al. 2006, ApJ, 642, 389

Pe'er, A., Ryde, F., Wijers, R. A. M. J., Mészáros, P., & Rees, M. J. 2007, ApJ, 664, L1

Piran, T. 2004, Reviews of Modern Physics, 76, 1143

Rees, M. J., & Meszaros, P. 1994, ApJ, 430, L93

Rhoads, J. E. 1999, ApJ, 525, 737

Sakamoto, T., Barthelmy, S. D., Baumgartner, W., et al. 2011, GRB Coordinates Network, 12276, 1

Sari, R., & Piran, T. 1999, ApJ, 520, 641

Sari, R., Piran, T., & Halpern, J. P. 1999, ApJ, 519, L17

Wang, F. Y., & Dai, Z. G. 2013, Nature Physics, 9, 465

Wang, F. Y., Dai, Z. G., Yi, S. X., & Xi, S. Q. 2015a, ApJS, 216, 8

Wang, X.-G., Zhang, B., Liang, E.-W., et al. 2015b, ApJS, 219, 9

Wei, J.-J., Wu, X.-F., Melia, F., Wei, D.-M., & Feng, L.-L. 2014, MNRAS, 439, 3329

Wu, X. F., Dai, Z. G., Huang, Y. F., & Lu, T. 2003, MNRAS, 342, 1131

Wu, X. F., Dai, Z. G., & Liang, E. W. 2004, ApJ, 615, 359

Wu, X. F., Dai, Z. G., Wang, X. Y., et al. 2007, Advances in Space Research, 40, 1208

Yi, S.-X., Wu, X.-F., & Dai, Z.-G. 2013, ApJ, 776, 120

Yi, S.-X., Wu, X.-F., Wang, F.-Y., & Dai, Z.-G. 2015, ApJ, 807, 92

Yi, S.-X., Lei, W.-H., Zhang, B., et al. 2017, Journal of High Energy Astrophysics, 13, 1

Yi, S.-X., Xi, S.-Q., Yu, H., et al. 2016, ApJS, 224, 20

Zhang, B., & Mészáros, P. 2004, International Journal of Modern Physics A, 19, 2385

Zhang, B., Fan, Y. Z., Dyks, J., et al. 2006, ApJ, 642, 354

Zhang, B., & Yan, H. 2011, ApJ, 726, 90

Zou, Y.-C., Cheng, K. S., & Wang, F. Y. 2015, ApJ, 800, L23

Zou, Y.-C., Fan, Y.-Z., & Piran, T. 2011, ApJ, 726, L2

Zou, Y.-C., & Piran, T. 2010, MNRAS, 402, 1854